Establishing Rod-Shape from Spherical, Peptidoglycan-Deficient Bacterial Spores

Huan Zhang[1], Garrett A. Mulholland[1], Sofiene Seef[2], Shiwei Zhu[3,4], Jun Liu[3,4], Tâm Mignot[2] and Beiyan Nan[1]*

[1]Department of Biology, Texas A&M University, College Station, TX 77843, USA
[2]Laboratoire de Chimie Bactérienne, CNRS - Université Aix Marseille UMR7283, Institut de Microbiologie de la Méditerranée, 13009 Marseille, France
[3]Department of Microbial Pathogenesis, Yale University School of Medicine, New Haven, CT 06536, USA
[4]Microbial Sciences Institute, Yale University, West Haven, CT 06516, USA

*Corresponding author: Beiyan Nan, 306C BSBE, 3258 TAMU, College Station, TX77843, Tel.: 979-845-3487, email: bnan@tamu.edu

Keywords: germination, Rod system, MreB, GTPase, gliding motor

ABSTRACT

Chemical-induced spores of the Gram-negative bacterium *Myxococcus xanthus* are peptidoglycan (PG)-deficient. It is unclear how these spherical spores germinate into rod-shaped, walled cells without preexisting PG templates. We found that germinating spores first synthesize PG randomly on spherical surfaces. MglB, a GTPase-activating protein, forms a cluster that surveys the status of PG growth and stabilizes at one future cell pole. Following MglB, the Ras family GTPase MglA localizes to the second pole. MglA directs molecular motors to transport the bacterial actin homolog MreB and the Rod PG synthesis complexes away from poles. The Rod system establishes rod-shape by elongating PG at nonpolar regions. Thus, the interaction between GTPase, cytoskeletons and molecular motors provides a mechanism for the *de novo* establishment of rod-shape in bacteria.

30 **Significance**

31 Spheres and rods are among the most common shapes adopted by walled bacteria, in which
32 the peptidoglycan (PG) cell wall largely determines cell shape. When induced by chemicals,
33 rod-shaped vegetative cells of the Gram-negative bacterium *Myxococcus xanthus* thoroughly
34 degrade their PG and shrink into spherical spores. As these spores germinate, rod-shaped cells
35 are rebuilt without preexisting templates, which provides a rare opportunity to visualize *de novo*
36 PG synthesis and bacterial morphogenesis. In this study, we investigated how spherical spores
37 germinate into rods and elucidated a system for rod-shape morphogenesis that includes the
38 Rod PG synthesis system, a GTPase-GAP pair, the MreB cytoskeleton and a molecular motor.

39 Morphogenesis is a fundamental feature of cells. Compared to spheres that are
40 symmetric in all directions, rods are asymmetric and polarized. For most rod-shaped
41 bacteria, the peptidoglycan (PG) cell wall defines cell geometry, which is assembled by
42 two major enzymatic systems. The Rod system consists of RodA, a SEDS-family PG
43 polymerase, PBP2, a member of the class B penicillin-binding proteins (bPBPs), and
44 MreB, a bacterial actin homolog that orchestrates the activities of the Rod complexes in
45 response to local cell curvature (1). In contrast, class A PBPs (aPBPs) contribute to PG
46 growth independent of MreB (2, 3).
47 *Myxococcus xanthus*, a rod-shaped Gram-negative bacterium, utilizes polarized
48 geometry for directed locomotion. MglA, a Ras family small GTPase, controls the
49 direction of gliding motility (4-7). As cells move, GTP-bound MglA forms large clusters at
50 leading cell poles, whereas GDP-bound MglA distributes homogeneously in the
51 cytoplasm (4, 6, 7). MglA-GTP stimulates the assembly of the gliding machineries
52 through direct interaction with MreB (7-10) and directs the gliding machineries toward
53 lagging cell poles (5). Consequently, the gliding machineries carry MreB filaments as
54 they move rapidly in the membrane (11-13). The activity of MglA is regulated by its
55 cognate GTPase-activating protein (GAP), MglB, which forms large clusters at lagging
56 cell poles. MglB activates the GTPase activity of MglA, expelling MglA-GTP, and thus
57 the assembled gliding machineries, from lagging poles (4, 6). Overall, polarized
58 localization and activities of MglA and MglB ensure that the of gliding machineries
59 generate propulsion by moving from poles to nonpolar regions (5, 7, 14).
60 Some rod-shaped bacteria change their geometry through sporulation. In
61 Firmicutes such as Bacilli and Clostridia, the morphological differentiation from rod-

62 shaped vegetative cells to oval spores begins with an asymmetric division, resulting in
63 the formation of a smaller endospore wholly contained within a larger mother cell. In
64 contrast to endospore-forming bacteria, *M. xanthus* produces spores using two division-
65 independent mechanisms. First, groups of vegetative cells can aggregate on solid
66 surfaces and build spore-filled fruiting bodies in a few days (15). Second, individual *M.*
67 *xanthus* cells can form dispersed, spherical spores within hours in response to chemical
68 signals, such as glycerol (16). Unlike endospores that contain intact and often thickened
69 PG (17, 18), PG is thoroughly degraded in glycerol-induced *M. xanthus* spores (19).
70 Without the polarity defined by PG, the mechanism by which these spores elongate into
71 rods remains largely unknown.

72 **Results**

73 **Two-phase morphological transition during *M. xanthus* spore germination.**

74 Overnight induction of wild-type cells by 1 M glycerol produced sonication-resistant
75 spores with length to width aspect ratios (L/W) of 1.56 ± 0.36 (n = 789), among which
76 40.9% are approximately spherical (L/W ≤ 1.3). Overall, the L/W values of most (85.4%)
77 spores were lower than 2. As spores germinated, the morphological transition
78 progressed in a two-phase manner. In the first hour (Phase I), L/W did not change
79 significantly (p = 0.57, Fig. 1A, 1B, *SI Appendix*, Movie S1, Table S1). After 1 h, L/W
80 increased sharply as emerging cells transformed into rods (Phase II). Importantly,
81 40.2% (n = 244) spores did not initiate elongation along their original long axes (Fig. 1C,
82 *SI Appendix,* Movie S2), indicating that although not perfectly spherical, the geometry of
83 mature spores does not predetermine the polarity of emerging cells. 70.2% (n = 198) of
84 emerging cells reached the dimensions of vegetative cells by 3 h. After 8 h, the whole
85 population of emerging cells is indistinguishable from vegetative cells (L/W = 5.55 ±
86 1.12, n = 233. Fig. 1A, 1B, *SI Appendix,* Movie S1, Table S1).

87 Using cryo-electron tomography (cryo-ET), we confirmed that mature glycerol-
88 induced spores do not retain PG (*SI Appendix,* Fig. S1). To investigate the role of PG
89 growth in germination, we treated spores with several inhibitors for PG assembly. In the
90 presence of A22, an inhibitor of MreB in the Rod system, spores failed to germinate into
91 rods as their L/W ratios did not increase within 8 h. In contrast, when the wild-type MreB
92 was replaced by $MreB^{V323A}$, an A22-resistant variant (9), spores were able to elongate
93 into rods in the presence of A22, indicating that A22 inhibits germination specifically
94 through MreB (Fig. 1A, 1B, *SI Appendix,* Table S1). Similarly, mecillinam that inhibits

95 PBP2 in the Rod system also blocked germination (Fig. 1A, 1B, *SI Appendix,* Table S1).
96 Both A22 and mecillinam-treated spores were viable because they were able to grow
97 into rods when transferred into inhibitor-free medium. Since these spores became even
98 more spherical in Phase I (Fig. 1D), neither A22 nor mecillinam blocked the hydrolysis
99 of spore coats that maintain the shape of oval spores. In the presence of cefsulodin that
100 inhibits PBP1A/B, and cefmetazole that inhibits all PBPs except PBP2, spores were
101 able to form rods, albeit the elongation rate was slower (Fig. 1A, 1B, *SI Appendix,* Table
102 S1). Although not essential for the initiation of cell elongation, aPBPs still contribute to
103 the maintenance of rod shape. Despite successful elongation in early Phase II (1 – 3 h),
104 57.2% (n = 215) cefsulodin-treated and 96.6% (n = 203) cefmetazole-treated emerging
105 cells retrogressed to spheres after 8-h treatments (Fig. 1A, 1B, *SI Appendix,* Table S1),
106 which is in agreement with a recent report that aPBPs are required for the mechanical
107 stability of cells (20). L/W values of the cefmetazole-treated spores increased
108 significantly in Phase I of germination ($p < 0.0001$, Fig. 1B, 1D, *SI Appendix,* Table S1),
109 suggesting that cells elongate earlier when PBP2 is dominant over other PBPs.
110 Vegetative *M. xanthus* cells are sensitive to fosfomycin, an antibiotic that inhibits the
111 production of UDP-MurNAc, a precursor of PG (11). As spores preserve PG precursors
112 (19), they were able to elongate into rods in the presence of fosfomycin, albeit at
113 reduced rates (Fig. 1A, 1B, *SI Appendix,* Table S1). Taken together, PG polymerization
114 by the Rod system is essential for the establishment of rod-shape.
115 Bacterial cells incorporate single D-amino acid-based fluorescent probes into PG
116 using D, D- and L, D-transpeptidases that catalyze the last steps of PG polymerization
117 (21). Such fluorescent D-amino acids could serve as proxy reporters for PG growth. We

118 next visualized the patterns of PG growth using a fluorescent D-amino acid, TAMRA 3-
119 amino-D-alanine (TADA) (22), to label newly synthesized PG. To enhance labeling
120 efficiency, we deleted the *dacB* gene (*mxan_3130*), which encodes a D-Ala-D-Ala
121 carboxypeptidase (23). The resulted *ΔdacB* cells showed identical morphology to the
122 wild-type ones and produced sonication-resistant spores. The *ΔdacB* spores showed
123 minor delay in germination and efficient TADA incorporation (Fig. 1E, *SI Appendix,* Fig.
124 S2 and Table S1). Although L/W of spores did not change in Phase I, PG had started to
125 grow. The surfaces of most Phase I spores (78.0%, n = 600) were evenly labeled by
126 TADA (Fig. 1E). The remaining 22.0% of spores showed bright patches of TADA on
127 their surfaces (Fig. 1F). However, these patches do not likely register future poles
128 because 47.0% (n = 132) of such spores contained more than two TADA patches and
129 these patches positioned randomly on spore surfaces (Fig. 1F, 1G). In contrast, as cells
130 grew into rods, TADA was incorporated heavily at nonpolar regions and fluorescence
131 signals were generally absent at cell poles (Fig. 1E). The patterns of PG growth indicate
132 that spores first synthesize PG on their spherical surfaces in Phase I and then break
133 symmetry in Phase II by growing PG at nonpolar regions.
134 Neither mecillinam, cefsulodin or cefmetazole was able to block TADA
135 incorporation in Phase I of germination. However, a treatment by all three antibiotics
136 abolished TADA incorporation (Fig. 1H), indicating that both aPBPs and the Rod system
137 contribute to the isotropic PG growth in Phase I. In contrast, mecillinam, but not
138 cefsulodin or cefmetazole, blocked TADA incorporation in Phase II of germination (Fig.
139 1H). The coordination between aPBPs and the Rod system still remains to be fully
140 understood. On the one hand, since cefsulodin and cefmetazole reduce the elongation

141 rates of emerging cells (Fig. 1A, 1B, *SI Appendix,* Table S1), aPBPs still participate in
142 PG synthesis in Phase II of germination. But on the other hand, the activities of aPBPs
143 might depend on the Rod system because mecillinam alone is sufficient to block TADA
144 incorporation in Phase II. Consistent with a recent report that cells reduce their diameter
145 when the Rod system becomes dominant over aPBPs (24), emerging cells continued to
146 grow in length but shrink in width in Phase II (Fig. S3, *SI Appendix,* Table S1). These
147 results confirm that while both aPBPs and the Rod system participate PG synthesis in
148 germination, the Rod system plays major roles in cell elongation.
149 **MglA and MglB are required for rapid cell elongation.** To investigate how *M. xanthus*
150 spores establish rod shape *de novo*, we tested the potential roles of polar-localized
151 motility regulators. *ΔmglA* and *ΔmglB* cells were able to form sonication-resistant spores
152 but their spores showed severe delays in elongation, especially in early Phase II of
153 germination. After 3 h, only 15.7% of the *ΔmglA* (n= 140) and 10.4% of *ΔmglB* (n = 298)
154 cells reached the vegetative aspect ratio (comparing to 70.2% of wild-type cells, Fig. 2A,
155 2B, *SI Appendix,* Table S1). In contrast, deleting *romR* and *plpA*, the genes encode two
156 additional polar-localized motility regulators (25-27), only caused minor delay in
157 germination (*SI Appendix,* Fig. S2 and Table S1). Both the *ΔmglA* and *ΔmglB* spores
158 were able to elongate in length and shrink in width, albeit at significantly lower rates
159 (Fig. 2A, 2B, *SI Appendix,* Table S1, Fig. S3), indicating that PG growth by the Rod
160 complex still occurred. Strikingly different from wild-type spores that maintained
161 relatively smooth cell surfaces during germination, cells from the *ΔmglA* and *ΔmglB*
162 spores showed pronounced bulges at nonpolar regions in early Phase II, appearing to
163 have multiple cell poles (Fig. 2A, 2C, *SI Appendix,* Movie S3). However, this

164 morphological defect was largely corrected after prolonged growth (8 h) (Fig. 2A),
165 implying that a system independent of MglA and MglB was able to generate rod shape,
166 although much less robustly. To determine how MglA and MglB regulate germination,
167 we investigated the spores that expressed the MglA^{Q82L} variant as the sole source of
168 MglA, under the control of the native promoter of the *mglBA* operon. MglA^{Q82L}
169 expresses normally but is unable to hydrolyze GTP (6). Spores expressing wild-type
170 MglB and MglA^{Q82L} showed both a severe delay in cell elongation and bulged surfaces
171 on emerging cells, similar to the *ΔmglA* and *ΔmglB* spores (Fig. 2A, 2B, *SI Appendix,*
172 Table S1). Surprisingly, overproducing MglB (*mglB^{OE}*), which potentially overstimulates
173 the GTPase activity of MglA, caused similar defects during germination (Fig. 2A, 2B, *SI*
174 *Appendix,* Table S1). Thus, fine-tuned GTPase activity of MglA is required for rapid cell
175 elongation and MglB functions through MglA.
176 Both the delayed morphological transition and bulged surfaces of the emerging
177 *ΔmglA* and *ΔmglB* cells suggest that MglA and MglB might regulate PG growth during
178 germination. *ΔmglA ΔdacB* and *ΔmglB ΔdacB* spores were able to grow PG in an
179 isotropic manner in Phase I, indistinguishable from the *ΔdacB* spores (Fig. 2D).
180 However, emerging cells from both mutant spores displayed elevated PG growth at cell
181 poles and bulges in Phase II (Fig. 2D).
182 Delayed elongation and uneven PG growth during germination could reduce the
183 viability of *ΔmglA* and *ΔmglB* spores, especially under osmotic stresses. To test this
184 hypothesis, we enumerated spores in cell-counting chambers and calculated their
185 viability by dilution plating. To simplify cell-counting, *pilA* was disrupted by plasmid
186 insertion (*pilA::tet*) to reduce cell aggregation caused by exopolysaccharides production

187 (28). As shown in Fig. 2E, compared to the *pilA::tet* spores that 88.9 ± 8.7% (calculated
188 from 3 independent experiments, same below) formed colonies, both *ΔmglA pilA::tet*
189 *and ΔmglB pilA::tet* spores formed colonies at reduced rates (54.1 ± 6.7 and 49.4 ±
190 12.9%, respectively). To further test if altered growth pattern reduces the strength of
191 PG, we allow spores to germinate for 1 h, then incubated emerging cells in a
192 hypoosmotic buffer (20 mM Tris-HCl, pH 7.6) for 1 h before plating. Hypoosmotic shock
193 reduced the survival rate of *pilA::tet* spores to 51.8 ± 2.6%, indicating that the still-
194 growing PG in germination Phase II is sensitive to osmotic stress. Strikingly, after
195 hypoosmotic shock, less than 15% of *ΔmglA pilA::tet* (14.5 ± 2.8%) and *ΔmglB pilA::tet*
196 (8.7 ± 2.4%) spores formed colonies (Fig. 2E). Taken together, the MglA-MglB polarity
197 axis regulates PG growth in Phase II of germination, which plays important roles in the
198 survival of glycerol-induced *M. xanthus* spores.
199 **MglB stabilizes at the first future pole**. We expressed YFP-labeled MglA as
200 merodiploids in the wild-type background (6, 9) and mCherry-labeled MglB (stably
201 expressed, *SI Appendix,* Table S1, Fig. S2) in the *ΔmglB* mutant and correlated their
202 localization patterns with germination progress (L/W). Spores from neither strain
203 showed significant defects in germination (*SI Appendix,* Table S1, Fig. S2). 94.1% (n =
204 152) of Phase I spores (L/W ≤ 2) contained one or two MglB clusters (Fig. 3A, 3B). In
205 phase II spores (L/W > 2), this ratio increased to 100% (n = 120). In contrast, MglA did
206 not form clusters until Phase II, when 54.2% of emerging cells contained one or two
207 MglA clusters (Fig. 3A, 3B). Thus, during germination, MglB establishes polarized
208 localization before MglA.

209 To test if the clusters of MglB in Phase I spores mark the polarity inherited from
210 previous vegetative cells, we imaged MglB clusters at 0.05 Hz. Surprisingly, the majority
211 of MglB clusters in Phase I spores was highly dynamic (Fig. 3C, *SI Appendix,* Movie
212 S4). Among 114 MglB clusters in Phase I spores, 22.9% remained stationary, and
213 77.1% showed typical diffusion, with diffusion coefficients (D_{MglB}) of $1.05 \times 10^{-4} \pm 4.62 \times$
214 10^{-5} $\mu m^2/s$. These "wandering" MglB clusters were observed in both the approximately
215 spherical (L/W < 1.3) and oval spores (1.3 < L/W ≤ 2), which supports our hypothesis
216 that, regardless of their geometry, polarity is not yet established in Phase I spores.
217 As germination progressed, MglB clusters started to stabilize. Strikingly, once
218 stabilized, the locations of MglB clusters became one of the cell poles for cell elongation
219 (Fig. 3D, *SI Appendix,* Movie. S5). In Phase II of germination (L/W > 2), the population
220 of stationary MglB clusters increased from 22.9% to 76.4% (n = 106, Fig. 3E). Stabilized
221 MglB clusters began to oscillate between newly established poles (Fig. 3C, *SI*
222 *Appendix,* Movie S6), which might provide a mechanism to ensure that MglB occupies
223 each future cell pole for an equal amount of time. As MglB clusters stabilized, MglA
224 started to form clusters. The formation of MglA-YFP clusters was delayed significantly in
225 the *ΔmglB* background, and only 23.3% (n = 120) of emerging cells contained MglA
226 clusters in Phase II of germination (Fig. 3A, 3B). Among the 204 cells in which both
227 proteins formed single clusters, 176 (86.3%) positioned MglA and MglB clusters at
228 opposite poles (Fig. 3A, 3B). Thus, spherical spores start to elongate into rods along the
229 axes established by the sequential stabilization of MglB and MglA clusters.
230 To investigate whether the stabilization of MglB clusters is predetermined by local
231 cell curvatures, we quantified the localization of stationary MglB clusters with regard to

232 the geometry of spores. We divide each spore/cell envelope into four quarters. In the
233 quarter that contained stationary MglB clusters, we defined the long and short axes as
234 0° and 90°, which mark the local curvature that shows the highest and lowest similarity
235 to the poles of vegetative cells, respectively. As shown in Fig. 3F, MglB clusters
236 stabilized randomly in Phase I spores, indicating that local curvature does not dictate
237 the localization of MglB. After the stabilization of MglB, the sites harboring MglB clusters
238 transformed into cell poles (0°) in Phase II (Fig. 3F).

239 MglB clusters could stabilize at the sites where PG synthesis has completed or not
240 yet initiated. We ruled out the second possibility because the majority of MglB clusters
241 (76.4%, n = 106) stabilizes at poles in Phase II (Fig. 3A, 3B), where almost no PG
242 growth was observed later (Fig. 1E). In Phase I of germination, the population of static
243 MglB clusters increased dramatically in the presence of A22, mecillinam, cefmetazole
244 and cefsulodin (Fig. 3E), indicating that active PG growth prevents MglB clusters from
245 settling down. Consistent with our finding that the Rod system becomes the dominant
246 system for PG growth in Phase II (Fig. 1H), A22 and mecillinam further reduced the
247 small population of diffusive MglB clusters in early Phase II, while cefmetazole and
248 cefsulodin did not show significant effects (Fig. 3E). Taken together, it is the progress of
249 PG growth, rather than the geometry of the spore, that regulates the dynamic of MglB
250 clusters. As MglB clusters only stabilize at the sites where PG growth is completed, a
251 region where PG synthesis completes first in Phase I will become a future cell pole.

252 **The MglA-MglB polarity axis regulates the distribution of the Rod system.** As the
253 Rod complex is the major system for PG growth in Phase II, the MglA-MglB polarity axis
254 might regulate cell elongation through the Rod complexes. However, MglA and MglB

255 are both cytoplasmic proteins, which are not likely to regulate the periplasmic activities
256 of the Rod system directly. To visualize the distribution of the Rod complexes, we fused
257 a DNA sequence encoding mCherry to the endogenous *rodA* gene in the wild-type
258 background. The resulted strain showed minor delay of elongation during sporulation
259 and was able to establish rod shape, indicating that the mCherry-labeled RodA retains
260 its enzymatic activity (*SI Appendix,* Fig. S2, Table S1). RodA-mCherry formed clusters
261 during both vegetative growth and germination (Fig. 4A). When imaged at 3.33 Hz,
262 RodA clusters showed typical diffusion in vegetative cells, with D_{RodA} = (3.07 ± 1.97) ×
263 10^{-2} $\mu m^2/s$ (n = 160) (*SI Appendix,* Movie. S7). Importantly, mecillinam treatment did not
264 affect the diffusivity of RodA clusters ((3.35 ± 2.14) × 10^{-2} $\mu m^2/s$, n = 58, p = 0.39) (*SI*
265 *Appendix,* Movie. S8), consistent with a previous report in *E. coli* that the diffusion of
266 PBP2 does not correlate with its catalytic activity (29). Despite its negligible effect on
267 diffusion, mecillinam significantly inhibited the formation of RodA clusters. During 150-s
268 of imaging at 0.33 Hz, untreated vegetative cells in the exponential phase formed 10.10
269 ± 3.41 RodA clusters/cell (n = 50). In the presence of mecillinam, this number
270 decreased to 3.06 ± 1.06 clusters/cell (n = 71) (Fig. 4A). Based on the above
271 observations, we reasoned that the formation of RodA clusters, rather than their
272 diffusion, correlates with PG growth by the Rod complexes.
273 To investigate whether MglA and MglB regulate the distribution of the Rod
274 complexes in Phase II of germination, we expressed RodA-mCherry endogenously in
275 *ΔmglA* and *ΔmglB* spores. Along the long axis of the emerging cells, we loosely defined
276 a region within 320 nm from each end of cell as a “pole” (which contains the cell pole
277 and its adjacent subpolar region) and the rest of the cell as the “nonpolar region”. In the

278 emerging cells from wild-type spores that expressed RodA-mCherry, the ratio between
279 nonpolar and polar-localized RodA clusters was 1.45 (n = 387, Fig. 4B). In contrast, in
280 the *ΔmglA* and *ΔmglB* backgrounds, this ratio decreased to 0.52 (n = 442) and 0.53 (n =
281 787), respectively (Fig. 4B). Our data support the hypothesis that during the sphere-to-
282 rod transition, the established MglA-MglB axis expels the Rod system from cell poles.
283 **The MglA-MglB polarity axis regulates the distribution of Rod complexes through**
284 **MreB and the gliding motor.** The diffusion of RodA and MglB clusters is not likely
285 connected. First, D_{RodA} is two orders of magnitude higher than D_{MglB}. Second, MglB only
286 diffuses in Phase I of germination while RodA diffuses during both germination and
287 vegetative growth. Thus, the MglA-MglB polarity axis does not likely regulate the
288 distribution of Rod complexes directly. Since MglA and the Rod complex both bind to
289 MreB, we hypothesized that the MglA-MglB polarity axis could regulate the distribution
290 of Rod complexes through MreB. Although a photoactivatable mCherry (PAmCherry)-
291 labeled MreB variant fully supports wild-type growth rate in vegetative cells (11), when
292 expressed as the sole source of MreB, it failed to support rapid cell elongation in Phase
293 II of germination. Nevertheless, spores expressing MreB-PAmCherry as merodiploids
294 showed wild-type germination kinetics (*SI Appendix,* Fig. S2, Table S1), which were
295 used to visualize the localization of MreB. When exposed to 405-nm excitation (0.2
296 kW/cm^2) for 2 s, the majority of PAmCherry was photoactivated (11, 13). MreB-
297 PAmCherry localized diffusively in Phase I spores, excluding the possibility that
298 localized MreB filaments predetermine the polarity of spores. MreB started to form small
299 patches in Phase II (Fig. 4C). Compared to the wild-type spores where MreB patches
300 mainly localized at nonpolar locations in germination Phase II, many MreB patches

301 formed near cell poles and bulges of the emerging *ΔmglA* and *ΔmglB* cells (Fig. 4C),
302 consistent with the altered distribution of RodA clusters. While MreB might localize at
303 bulges in response to altered local cell curvatures in these mutants (30-35), the
304 aggregation of MreB at their poles is more likely due to the loss of the MglA-MglB
305 polarity axis, because the poles of both wild-type and mutant cells have similar
306 curvatures.

307 MglA connects MreB to the gliding motors and the gliding motors drive the
308 movement of MreB filaments (5, 7, 11). To test if MglA recruits the gliding motors to
309 transport the Rod complexes to nonpolar locations through MreB, we investigated the
310 regrowth process of the *ΔaglQS* pseudospores that are sonication-sensitive due to the
311 lack compact polysaccharide layers on their surfaces (36). *ΔaglQS* cells carry truncated
312 gliding motors that are unable to drive the rapid motion of MreB filaments (11).
313 Phenocopying the *ΔmglA* and *ΔmglB* spores, elongation of *ΔaglQS* pseudospores
314 delayed significantly (Fig. 2A, 2B). Many emerging *ΔaglQS* cells displayed bulged
315 surfaces in Phase II and survived at reduced rate, especially after hypoosmotic shock
316 (Fig. 2A, 2E). Consistently, significantly higher PG growth was observed at cell poles
317 and bulges in the elongation phase, similar to the observation made in *ΔmglA ΔdacB*
318 and *ΔmglB ΔdacB* spores (Fig. 2D). Accordingly, significantly higher fractions of RodA
319 clusters and MreB filaments were observed at poles and bulges in elongating *ΔaglQS*
320 cells (Fig. 4B, 4C). In summary, MglA and MglB restrict PG growth to nonpolar regions
321 in germination Phase II utilizing the gliding motors, which transport MreB, and thus the
322 whole Rod complexes, under the control of MglA.

323 **Discussion**

324 As spheres and rods are among the most common shapes adopted by walled bacteria,
325 the sphere-to-rod transition during *M. xanthus* spore germination provides a unique
326 opportunity to study rod-like morphogenesis in bacteria. Due to the absence of PG,
327 glycerol-induced *M. xanthus* spores are especially valuable for the study of *de novo* PG
328 synthesis, which drives spontaneous cell elongation in homogenous environments. We
329 observed that MglB forms wandering clusters in Phase I of germination and that an
330 emerging cell starts to elongate when the MglB cluster stops moving and stabilizes at
331 what is to become a future pole. The dynamics of MglB clusters is sensitive to the status
332 of PG synthesis because active PG growth prevents MglB clusters from settling down.
333 Since MglB avoids colocalizing with MglA-GTP by converting the latter to MglA-GDP (4,
334 6), and MglA-GTP binds to MreB (which also carries the Rod complexes) (7), MglB
335 clusters cannot stabilize at the sites where active PG synthesis by the Rod complex
336 occurs. We propose that the wandering dynamics of MglB clusters serves as a
337 mechanism to survey the status of PG growth and the region where PG growth
338 completes first in Phase I will host a MglB cluster and become a future pole in Phase II
339 (Fig. 5). Once an MglB cluster stabilizes at one pole, the expulsion between MglB and
340 MglA-GTP causes MglA-GTP to cluster at the opposite side of the spore. At the poles
341 that contain MglB clusters, MglB expels MglA-GTP and thus the Rod complexes from
342 the poles. At the opposite poles, MglA-GTP stimulates the assembly of the gliding
343 machinery by directly connecting it to MreB (7, 14). Once assembled, the gliding
344 machineries transport MreB filaments, thus entire Rod complexes, away from the poles
345 (5, 11) (Fig. 5). Taken together, the diametrically opposing clusters of MglA-GTP and

346 MglB establish the polarity axis of the emerging cell, which restricts the activity of the
347 Rod complex to nonpolar locations (Fig. 5). Other regulators that modulate the gliding
348 motors, such as PlpA and RomR, could also connect to the Rod system through MreB,
349 and thus respond to the status of PG synthesis. Utilizing the same system that defines
350 the leading-lagging axis in vegetative cells, spherical spores grow their walls at nonpolar
351 regions and eventually form rods.

352 Our findings suggest that multiple factors contribute to the establishment of rod
353 shapes, among which the MglA-MglB polarity axis plays a prominent role. In the
354 absence of MglA and MglB, other polarity regulators, including PlpA and RomR that
355 also regulate the gliding motors, and potentially asymmetrically-localizes cellular
356 components such as to-be-identified germinant receptors, ribosomes and RNA
357 polymerase, still drive cell elongation, albeit much slower. Understanding these failsafe
358 mechanisms will pave the way for fully understanding the mechanism of rod-like
359 morphogenesis. The mechanism by which the gliding machineries facilitate both gliding
360 and PG growth remains to be investigated. Nonetheless, our results have added
361 another layer to the striking versatility of the gliding motors, which transport various
362 cargos in different compartments of the cells: spore coats on cell surfaces (36), the Rod
363 complex and some gliding proteins in the membrane and periplasm (12, 14), as well as
364 MreB and other gliding proteins in the cytoplasm (11, 14, 37).

365 **Materials and Methods**

366 **Strain construction.** Deletion and insertion mutants were constructed by
367 electroporating *M. xanthus* cells with 4 μg plasmid DNA or 1 μg of chromosomal DNA.
368 Transformed cells were plated on CYE plates supplemented with 100 μg/ml sodium
369 kanamycin sulfate or 10 μg/ml tetracycline hydrochloride. In-frame deletion of *dacB* is
370 described in *SI Appendix, Materials and Methods, Table S2.*

371 **Sporulation, spore purification and germination.** Vegetative *M. xanthus* cells were
372 grown in liquid CYE medium (10 mM MOPS pH 7.6, 1% (w/v) Bacto™ casitone (BD
373 Biosciences), 0.5% yeast extract and 4 mM $MgSO_4$) at 32 °C, in 125-ml flasks with
374 rigorous shaking, or on CYE plates that contains 1.5% agar. When liquid cell culture
375 reaches OD_{600} 0.1 – 0.2, glycerol was added to 1 M to induce sporulation. After rigorous
376 shaking overnight at 32 °C, remaining vegetative cells were eliminated by sonication
377 and sonication-resistant spores were purified by centrifugation (1 min, 15,000 g and
378 4 °C). The pellet was washed three times with water. More details of spore purification
379 and the purification of *ΔaglQS* pseudospores are provided in *SI Appendix, Materials and*
380 *Methods.*

381 **Microscopy Analysis.** Cryo-ET was performed on a Polara G2™ electron microscope.
382 Images were collected at 9,000× magnification and 8-μm defocus, resulting in 0.42
383 nm/pixel. Data were acquired automatically with the SerialEM software (38). Time-lapse
384 videos of the germination progress of wild-type and *ΔmglA* spores were recorded using
385 an OMAX™ A3590U CCD camera and a Plan Flour™ 40×/0.75 Ph2 DLL objective on a
386 phase-contrast Nikon Eclipse™ 600 microscope. The length, width and geometric
387 aspect ratios (L/W) of spores/cells were determined from differential interference

388 contrast (DIC) images using a custom algorithm written in MATLAB (The MathWorks,
389 Inc., Natick, MA), which is available upon request. DIC images of spores/cells were
390 captured using a Hamamatsu ImagEM X2™ EM-CCD camera C9100-23B (effective
391 pixel size 160 nm) on an inverted Nikon Eclipse-Ti™ microscope with a 100× 1.49 NA
392 TIRF objective, which are also used for capturing fluorescence images. MglB and RodA
393 clusters were localized using an algorithm written in MATLAB (11), which is available
394 upon request. More detailed information is provided in *SI Appendix, Materials and*
395 *Methods.*

References

1. S. van Teeffelen, L. D. Renner, Recent advances in understanding how rod-like bacteria stably maintain their cell shapes. *F1000Res* **7**, 241 (2018).
2. H. Cho *et al.*, Bacterial cell wall biogenesis is mediated by SEDS and PBP polymerase families functioning semi-autonomously. *Nat Microbiol* 10.1038/nmicrobiol.2016.172, 16172 (2016).
3. T. K. Lee, K. Meng, H. Shi, K. C. Huang, Single-molecule imaging reveals modulation of cell wall synthesis dynamics in live bacterial cells. *Nature communications* **7**, 13170 (2016).
4. S. Leonardy *et al.*, Regulation of dynamic polarity switching in bacteria by a Ras-like G-protein and its cognate GAP. *Embo J* **29**, 2276-2289 (2010).
5. B. Nan *et al.*, The polarity of myxobacterial gliding is regulated by direct interactions between the gliding motors and the Ras homolog MglA. *Proc Natl Acad Sci U S A* **112**, E186-193 (2015).
6. Y. Zhang, M. Franco, A. Ducret, T. Mignot, A bacterial Ras-like small GTP-binding protein and its cognate GAP establish a dynamic spatial polarity axis to control directed motility. *PLoS Biol* **8**, e1000430 (2010).
7. A. Treuner-Lange *et al.*, The small G-protein MglA connects to the MreB actin cytoskeleton at bacterial focal adhesions. *J Cell Biol* **210**, 243-256 (2015).
8. B. Nan, M. J. McBride, J. Chen, D. R. Zusman, G. Oster, Bacteria that glide with helical tracks. *Curr Biol* **24**, R169-R173 (2014).
9. E. M. Mauriello *et al.*, Bacterial motility complexes require the actin-like protein, MreB and the Ras homologue, MglA. *Embo J* **29**, 315-326 (2010).
10. B. Nan, Bacterial Gliding Motility: Rolling Out a Consensus Model. *Curr Biol* **27**, R154-R156 (2017).
11. G. Fu *et al.*, MotAB-like machinery drives the movement of MreB filaments during bacterial gliding motility. *Proc Natl Acad Sci U S A* **115**, 2484-2489 (2018).
12. B. Nan *et al.*, Myxobacteria gliding motility requires cytoskeleton rotation powered by proton motive force. *Proc Natl Acad Sci U S A* **108**, 2498-2503 (2011).
13. B. Nan *et al.*, Flagella stator homologs function as motors for myxobacterial gliding motility by moving in helical trajectories. *Proc Natl Acad Sci U S A* **110**, E1508-1513 (2013).
14. L. M. Faure *et al.*, The mechanism of force transmission at bacterial focal adhesion complexes. *Nature* **539**, 530-535 (2016).
15. D. R. Zusman, A. E. Scott, Z. Yang, J. R. Kirby, Chemosensory pathways, motility and development in *Myxococcus xanthus*. *Nat Rev Microbiol* **5**, 862-872 (2007).
16. M. Dworkin, S. M. Gibson, A System for Studying Microbial Morphogenesis: Rapid Formation of Microcysts in *Myxococcus xanthus*. *Science* **146**, 243-244 (1964).
17. E. I. Tocheva *et al.*, Peptidoglycan transformations during *Bacillus subtilis* sporulation. *Mol Microbiol* **88**, 673-686 (2013).
18. K. Khanna *et al.*, The molecular architecture of engulfment during *Bacillus subtilis* sporulation. *Elife* **8** (2019).

441 19. N. K. Bui *et al.*, The peptidoglycan sacculus of *Myxococcus xanthus* has unusual
442 structural features and is degraded during glycerol-induced myxospore
443 development. *J Bacteriol* **191**, 494-505 (2009).
444 20. A. Vigouroux *et al.*, Class-A penicillin binding proteins do not contribute to cell
445 shape but repair cell-wall defects. *Elife* **9** (2020).
446 21. E. Kuru *et al.*, Mechanisms of incorporation for D-amino acid probes that target
447 peptidoglycan biosynthesis. *ACS Chem Biol* 10.1021/acschembio.9b00664
448 (2019).
449 22. Y. P. Hsu *et al.*, Full color palette of fluorescent d-amino acids for in situ labeling
450 of bacterial cell walls. *Chem Sci* **8**, 6313-6321 (2017).
451 23. E. Kuru *et al.*, In Situ probing of newly synthesized peptidoglycan in live bacteria
452 with fluorescent D-amino acids. *Angew Chem Int Ed Engl* **51**, 12519-12523
453 (2012).
454 24. M. F. Dion *et al.*, *Bacillus subtilis* cell diameter is determined by the opposing
455 actions of two distinct cell wall synthetic systems. *Nat Microbiol* 10.1038/s41564-
456 019-0439-0 (2019).
457 25. D. Keilberg, K. Wuichet, F. Drescher, L. Sogaard-Andersen, A response
458 regulator interfaces between the Frz chemosensory system and the MglA/MglB
459 GTPase/GAP module to regulate polarity in *Myxococcus xanthus*. *PLoS Genet* **8**,
460 e1002951 (2012).
461 26. C. B. Pogue, T. Zhou, B. Nan, PlpA, a PilZ-like protein, regulates directed motility
462 of the bacterium *Myxococcus xanthus*. *Mol Microbiol* **107**, 214-228 (2018).
463 27. Y. Zhang, M. Guzzo, A. Ducret, Y. Z. Li, T. Mignot, A dynamic response regulator
464 protein modulates G-protein-dependent polarity in the bacterium *Myxococcus*
465 *xanthus*. *PLoS Genet* **8**, e1002872 (2012).
466 28. T. Zhou, B. Nan, Exopolysaccharides promote *Myxococcus xanthus* social
467 motility by inhibiting cellular reversals. *Mol Microbiol* **103**, 729-743 (2017).
468 29. T. K. Lee *et al.*, A dynamically assembled cell wall synthesis machinery buffers
469 cell growth. *Proc Natl Acad Sci U S A* **111**, 4554-4559 (2014).
470 30. B. P. Bratton, J. W. Shaevitz, Z. Gitai, R. M. Morgenstein, MreB polymers and
471 curvature localization are enhanced by RodZ and predict *E. coli*'s cylindrical
472 uniformity. *Nature communications* **9**, 2797 (2018).
473 31. A. Colavin, H. Shi, K. C. Huang, RodZ modulates geometric localization of the
474 bacterial actin MreB to regulate cell shape. *Nature communications* **9**, 1280
475 (2018).
476 32. S. Hussain *et al.*, MreB filaments align along greatest principal membrane
477 curvature to orient cell wall synthesis. *Elife* **7** (2018).
478 33. T. S. Ursell *et al.*, Rod-like bacterial shape is maintained by feedback between
479 cell curvature and cytoskeletal localization. *Proc Natl Acad Sci U S A* **111**,
480 E1025-1034 (2014).
481 34. F. Wong, E. C. Garner, A. Amir, Mechanics and dynamics of translocating MreB
482 filaments on curved membranes. *Elife* **8** (2019).
483 35. R. M. Morgenstein *et al.*, RodZ links MreB to cell wall synthesis to mediate MreB
484 rotation and robust morphogenesis. *Proc Natl Acad Sci U S A*
485 10.1073/pnas.1509610112 (2015).

36. M. Wartel *et al.*, A versatile class of cell surface directional motors gives rise to gliding motility and sporulation in *Myxococcus xanthus*. *PLoS Biol* **11**, e1001728 (2013).
37. M. Sun, M. Wartel, E. Cascales, J. W. Shaevitz, T. Mignot, Motor-driven intracellular transport powers bacterial gliding motility. *Proc Natl Acad Sci U S A* **108**, 7559-7564 (2011).
38. D. N. Mastronarde, Automated electron microscope tomography using robust prediction of specimen movements. *Journal of Structural Biology* **152**, 36-51 (2005).

496 **ACKNOWLEDGEMENTS**

497 We thank Autumn Ridge and Elias Topo for technical assistance, Drs. Joseph Sorg and
498 Ritu Shrestha for their help in the initial determination of germination phenotypes, Drs.
499 Michael Van Nieuwenhze and Yen-Pang Hsu for providing TADA, and Drs. David
500 Zusman, Michael Manson and Joseph Sorg for critical reading of this manuscript. This
501 work is supported by the National Institute of Health R01GM129000 (to B.N.) and
502 R01AI087946 (to J.L.) and by CNRS to T.M.

503 **Figures**

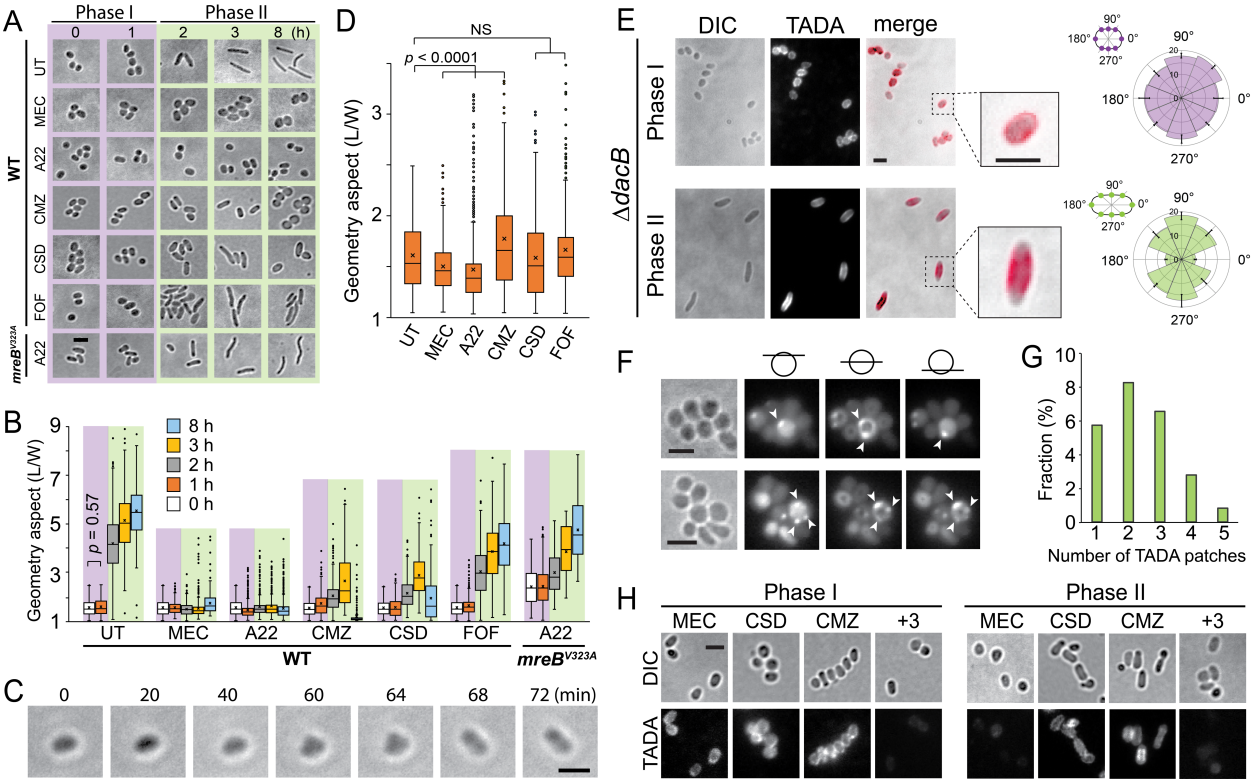

504

505 **Fig. 1. PG polymerization by the Rod system is essential for *de novo***

506 **establishment of rod-shape. A)** Morphological changes of untreated (UT) and

507 inhibitor-treated spores in the germination process. A22 (10 μg/ml), mecillinam (MEC,

508 100 μg/ml), cefmetazole (CMZ, 5 mg/ml), cefsulodin (CSD, 5 mg/ml) and fosfomycin

509 (FOF, 8 mg/ml). **B)** Quantitative analysis of the germination progress using the aspect

510 ratios (L/W) of spores/cells. Boxes indicate the 25th - 75th percentiles, whiskers the 5th -

511 95th percentiles. In each box, the midline indicates the median and × indicates the mean

512 (same below, Table S1). Outlier data points are shown as individual dots above and

513 below the whiskers. **C)** An oval spore initiates elongation along its short axes (Movie

514 S2). **D)** Phase I spores become more spherical after 1-h treatments by A22 and

515 mecillinam. Cefmetazole-treated spores initiate elongation earlier than untreated ones.

516 **E)** Patterns of PG growth in both phases of germination were visualized by TADA in
517 *ΔdacB* spores. The average and standard deviation of TADA intensity were calculated
518 from 20 spores/cells in the diagrams to the right (same below). **F)** Imaged at different
519 focal planes, 22.0% of Phase I spores show bright TADA patches (arrows) that position
520 randomly on spore surfaces. **G)** Among these 22.0% spores, many contain multiple
521 TADA patches. **H)** Compared to untreated (UT) *ΔdacB* spores, while neither MEC, CMZ
522 or CSD is able to block PG growth, the combination of all three antibiotics (+3)
523 abolishes PG growth in Phase I of germination. In contrast, MEC alone is sufficient to
524 inhibit PG growth in Phase II. Scale bars, 2 μm. *p* values were calculated using the
525 Student paired *t* test with a two- tailed distribution (same below). NS, nonsignificant
526 difference.

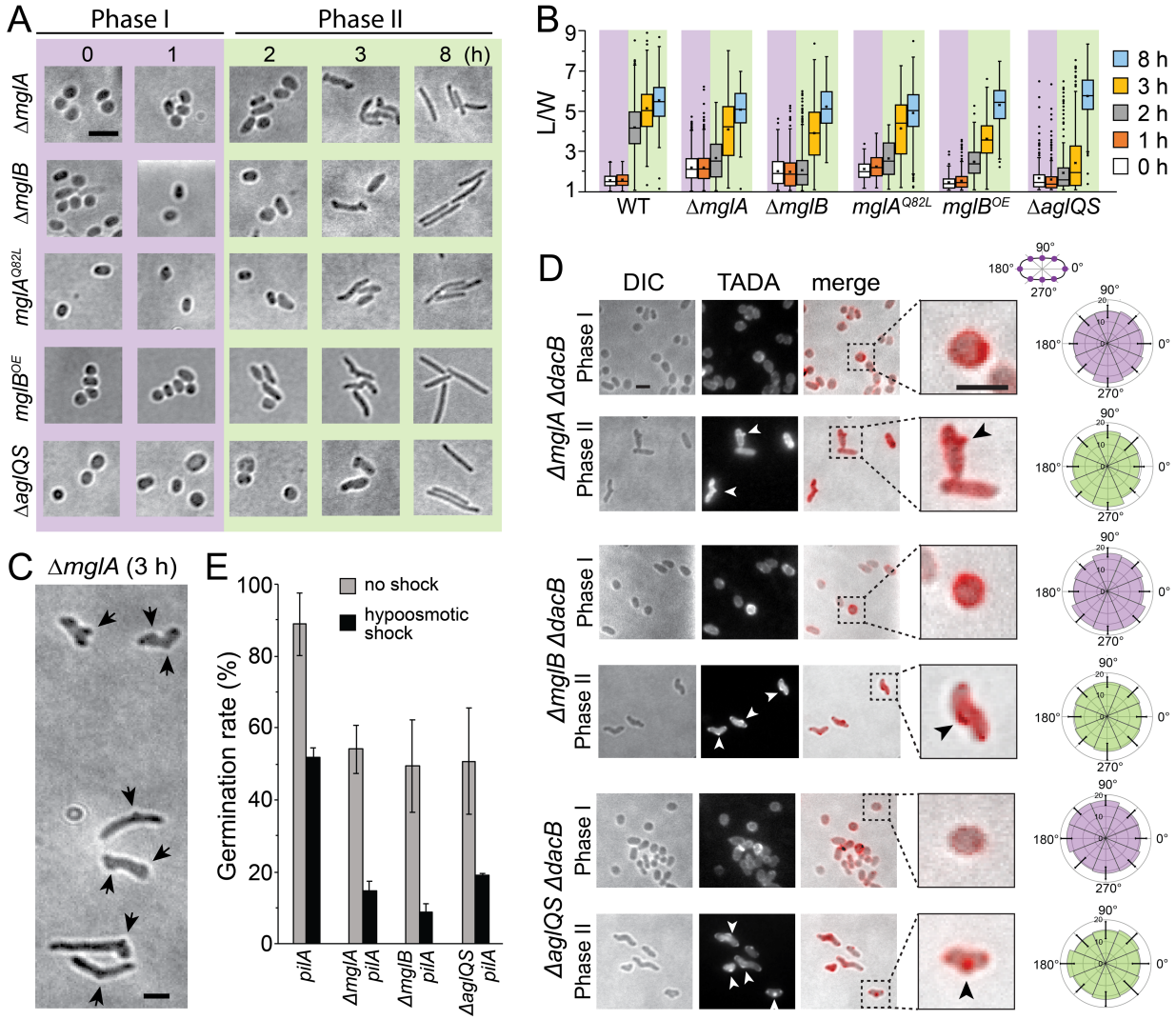

Fig. 2. MglA and MglB are required for rapid cell elongation. A) Emerging cells from *ΔmglA*, *ΔmglB, mglA*^{Q82L} and *mglB*^{OE} spores and *ΔaglQS* pseudospores show significant delay in elongation and bulges on cell surfaces in Phase II of germination. **B)** Quantitative analysis of the germination progress. **C)** A representative image of the altered morphology of the emerging *ΔmglA* cells after 3-h of germination. Arrows point to the bulges on cell surfaces. **D)** The disruption of either the MglA-MglB polar axis (*ΔmglA ΔdacB* and *ΔmglB ΔdacB*) or the gliding motor (*ΔaglQS ΔdacB*) resulted in significantly stronger PG growth at cell poles and budges (arrows) in Phase II.

536 Quantitative analysis of TADA fluorescence is shown on the right. **E)** The disruption of
537 either the MglA-MglB polar axis (*ΔmglA pilA::tet* and *ΔmglB pilA::tet*) or the gliding motor
538 (*ΔaglQS pilA::tet*) significantly decreases the survival rate of germinating spores (gray
539 bars), especially under osmotic stress (black bars). Scale bars, 2 μm.

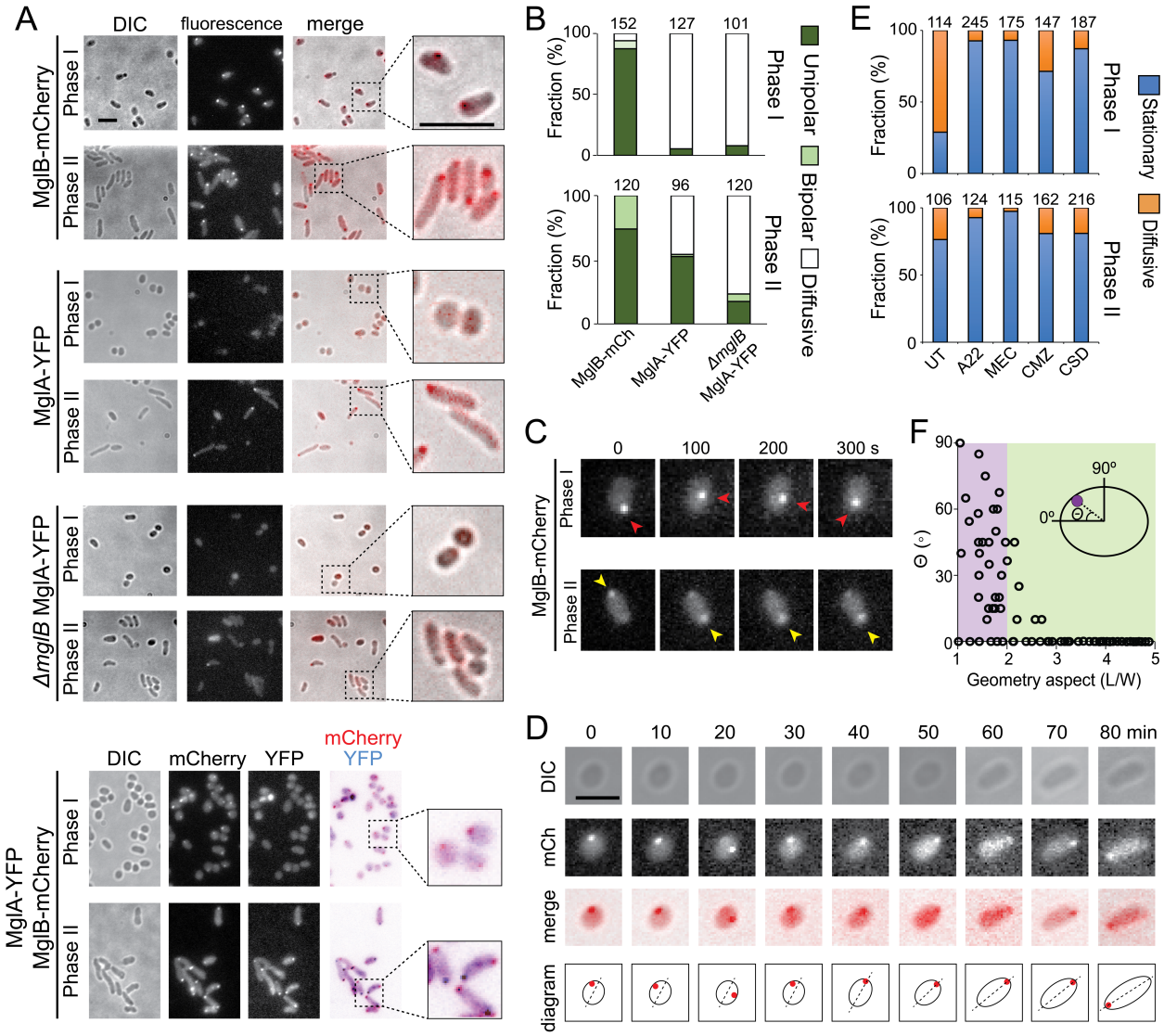

Fig. 3. MglB stabilizes at the first future pole. A) While MglB-mCherry forms clusters in germination Phase I, MglA-YFP starts to forms clusters in Phase II. In the absence of MglB, MglA-YFP forms significantly fewer clusters. MglA and MglB clusters stabilize at opposite cell poles. **B)** Quantification of the sequential stabilization of MglB and MglA clusters. The total number of spores/cells analyzed for each strain is shown on top of each bar. **C)** The "wandering" dynamics of MglB clusters (red arrow) in Phase I spores (Movie S4). In Phase II, MglB clusters (yellow arrow) stabilized at cell poles and oscillated between opposite poles (Movie S6). **D)** As the MglB cluster stabilizes at one

549 future pole, the emerging cell starts to elongate (Movie S5). **E)** Inhibitors of PG
550 synthesis, A22, MEC, CMZ and CSD, all inhibit the wandering of MglB in Phase I. In
551 contrast, only A22 and MEC, the inhibitors of the Rod system, inhibit the wandering of
552 MglB significantly in Phase II. For each treatment, the total number of MglB clusters
553 analyzed is shown on top of each bar. UT, untreated. **F)** The stabilization of MglB
554 clusters does not depend on local curvature. Scales bars, 2 μm.

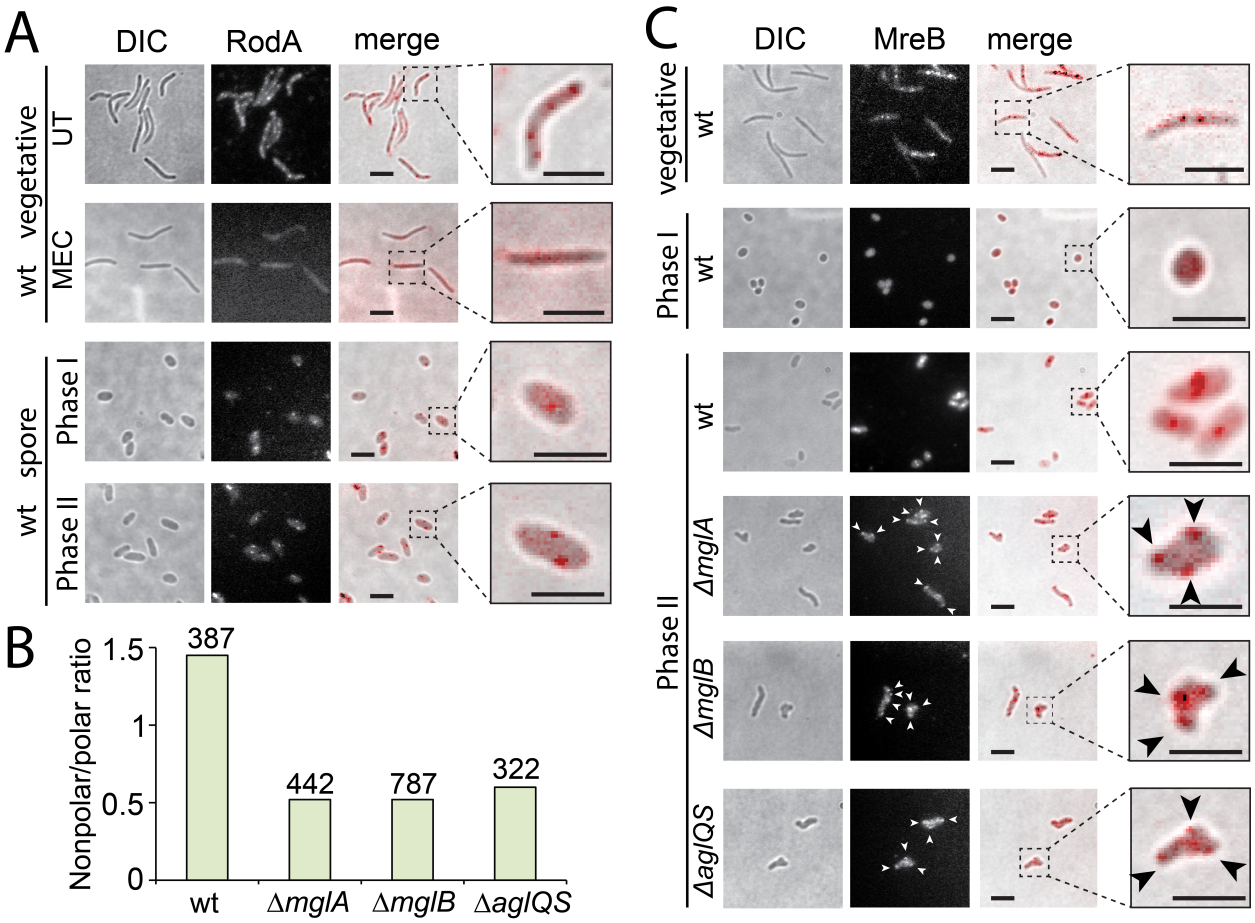

Fig. 4. The MglA-MglB polarity axis regulates the distribution of Rod complexes through MreB and the gliding motor. A) RodA forms clusters during both vegetative growth and germination. Mecillinam reduces the formation of RodA clusters in vegetative cells. **B)** Nonpolar-to-polar distribution ratios of RodA clusters in the elongating cells of germination Phase II. The total number of RodA clusters analyzed is shown on top of each bar. **C)** The localization patterns of MreB filaments. Consistent with the altered distribution of RodA cluster, MreB patches (arrows) are frequently detected near cell poles and bulges in the emerging *ΔmglA*, *ΔmglB* and *ΔaglQS* cells in Phase II of germination. Scales bars, 2 μm

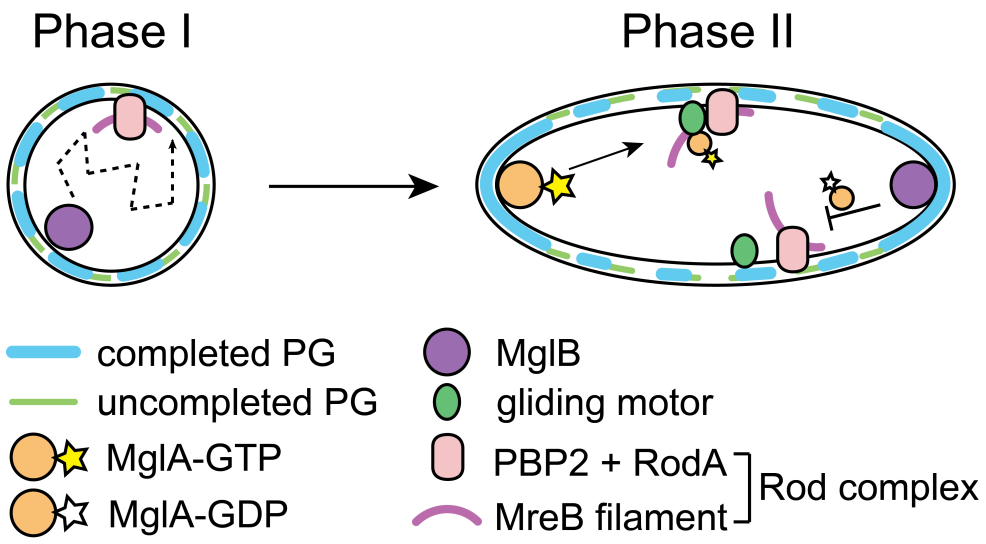

Fig.5. A schematic model for the *de novo* establishment of rod-shape by the MglA-MglB polarity axis.